ACS APPLIED MATERIALS & INTERFACES

Research Article

www.acsami.org

Near-Infrared Light Manipulated Chemoselective Reductions Enabled by an Upconversional Supersandwich Nanostructure

Zi-en Liu,[†,‡] Jie Wang,[†] Yan Li,[†] Xiaoxia Hu,[†] Junwen Yin,[†] Yeqing Peng,[†] Zhihao Li,[†] Yawen Li,[†] Baomin Li,[‡] and Quan Yuan*[,†]

[†]Key Laboratory of Analytical Chemistry for Biology and Medicine (Ministry of Education), College of Chemistry and Molecular Sciences, Wuhan University, Wuhan 430072, China

[‡]School of Chemistry Engineering and Technology, China University of Mining and Technology, Xuzhou 221008, China

Supporting Information

ABSTRACT: Core−satellite is one of the most powerful superstructures since it leads to enhanced or completely new properties through compatible combination of each component. Here we create a novel ceria-based core−shell−satellite supersandwich structure with near-infrared (NIR) light manipulated catalytic activity by integrating the upconversion luminescent and catalytic functionality of CeO_2 nanoparticles. Specifically, lanthanide-doped octahedral CeO_2 nanoparticles (o-CeO_2) are coated with silica layer (o-CeO_2@SiO_2) to enhance their luminescence intensity. The pH-dependent catalytic active cubic CeO_2 nanoparticles (c-CeO_2) are then assembled on the surface of o-CeO_2@SiO_2 to form the supersandwich structure (o-CeO_2@SiO_2@c-CeO_2) following a classic chemical reaction. The upconversion quantum yield of o-CeO_2 in this nanostructure can be nearly doubled. Furthermore, under NIR light irradiation, the o-CeO_2@SiO_2@c-CeO_2 supersandwich structure based composite catalyst displays superior catalytic activity in selective reduction of aromatic nitro compounds to corresponding azo compounds, and the composite photocatalyst can be easily recycled for several times without significant loss of catalytic activity. This strategy may serve as a universal method for the construction of multifunctional nanostructures and shed light on the green chemistry for chemical synthesis.

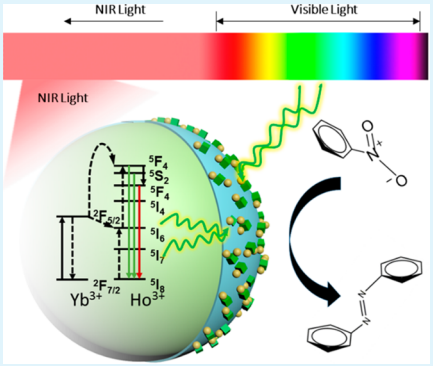

KEYWORDS: *cerium oxide, upconversion, photocatalysis, near-infrared light, green chemistry*

INTRODUCTION

In the past several decades, nanomaterials have attracted much attention from a wide spectrum of scientific communities because their properties (luminescence,[1−3] catalysis,[4,5] and so on) are significantly different from those of their bulk counterparts.[6,7] Developing nanomaterials with superstructures and multiple functions is one of the most popular research areas in materials science since these materials are more appropriate to meet the challenges in fields such as green catalysis,[8−10] bioimaging,[11] and drug delivery.[12] Among all of the intriguing nanostructures, core−satellite structure holds great potential because of its easy fabrication and integration of the properties of different components at the nanoscale, so that enhanced or completely new properties are obtained.[13−15] Through rational design, core and satellite components in the core−satellite structure can elicit synergistic activities and thus can realize applications that cannot be accomplished with other monofunctional materials.

Cerium oxide (CeO_2) has gained more and more research interest in recent years for its superb redox properties and extensive applications in areas such as CO oxidation[16] and water−gas shift reaction.[17] One of the most outstanding properties of CeO_2 is its special redox capability, which originates from the reversible transformation between Ce^{3+} and Ce^{4+}.[18,19] Normally, CeO_2 nanoparticles with reduced sizes possess much stronger redox capabilities and greater catalytic activities due to largely increased surface defects and surface to volume ratio.[20−22] Beyond that, due to the special chemical and thermal stabilities of CeO_2, small CeO_2 nanoparticles can also serve as excellent catalyst carriers with performance comparable to or even superior than bulk CeO_2 according to previous studies.[16]

Recently, lanthanide-doped upconversion nanomaterials have attracted much attention for their intriguing ability to absorb two or more photons and then emit light at wavelength shorter than the excitation wavelength.[23] Apart from superb redox property and good performance as catalyst carriers, CeO_2 may also serve as potential matrix material in lanthanide-doped phosphors[24−27] since it exhibits good charge transfer abilities.[28,29] During the past several years, CeO_2 based upconversion nanomaterials have rarely been explored due to their relatively low quantum yields caused by the surface

Received: June 24, 2015
Accepted: August 13, 2015
Published: August 13, 2015

DOI: 10.1021/acsami.5b05633
ACS Appl. Mater. Interfaces 2015, 7, 19416−19423

quenching effect in part. Since several methods have been well established to enhance the luminescent intensities of nanophosphors,[30] such as coating the nanoparticles with a layer of inert shell,[31,32] thus CeO_2 can also act as prominent matrix material in the fabrication of novel upconversion luminescent materials. Herein, we have rationally developed a novel CeO_2-based core−shell−satellite supersandwich structure that integrates upconversion luminescent and catalytic functions within a single nanoparticle. Specifically, large octahedral CeO_2 nanoparticles doped with lanthanide ions (designated as o-CeO_2) were uniformly coated with a layer of silica shell (designated as o-CeO_2@SiO_2) to improve their luminescent quantum yields by passivating the surface defects and providing ligand fields. Undoped small cubic CeO_2 nanoparticles (designated as c-CeO_2) with excellent catalytic capabilities were assembled on the surface of o-CeO_2@SiO_2 to construct the core−shell−satellite supersandwich structure (designated as o-CeO_2@SiO_2@c-CeO_2) with the aid of the well-known EDC/NHS chemistry. It is noteworthy that the quantum yield of CeO_2 based upconversion luminescent nanomaterials was nearly doubled. Furthermore, the core−shell-satellite nanoparticles were loaded with gold nanoparticles (designated as o-CeO_2@SiO_2@c-CeO_2/Au), and the performance of the resultant nanocomposites in selectively catalytic conversion of aromatic nitro compounds into corresponding azo compounds under near-infrared (NIR) light irradiation was encouraging. More excitingly, the composite catalyst can be easily recycled several times while retaining effectiveness. The strategy described here not only may further promote the applications of ceria based materials in areas such as bioimaging, biomedicine, and photocatalysis, but also can serve as a universal method for construction of multifunctional materials for other complicated applications.

EXPERIMENTAL SECTION

Synthesis of o-CeO_2. Octahedral ceria nanoparticles were synthesized according to a previously reported method.[33] Typically, 0.4875 g of $Ce(NO_3)_3{\cdot}6H_2O$, 0.5 g of polyvinylpyrrolidone (PVP-3000), and certain amount of $Ln(NO_3)_3$ solution (0.2 M) were dissolved in the mixture of deionized (DI) water (30 mL) and anhydrous ethanol (10 mL). Then the as prepared solution was stirred for 30 min and transferred into a 50 mL Teflon-lined steel autoclave. The solution was heated to 160 °C and was allowed to react for 24 h. After cooling to room temperature, the solution was centrifuged and the obtained nanoparticles were washed with ethanol for 3 times. The resultant nanoparticles was dried at 60 °C overnight and then calcined at 600 °C for 4 h.

Synthesis of c-CeO_2. Tiny CeO_2 nanocubes were synthesized by the classic solvothermal reactions.[34] Powders of $(NH_4)_2Ce(NO_3)_6$ (2.74 g) and CH_3COONa (10 g) were dissolved 70 mL of DI water, and then 10 mL of CH_3COOH was added. After stirring at room temperature for 1 h, the obtained slurry was transferred in a Teflon-lined steel autoclave and treated at 220 °C to react for 12 h. After this hydrothermal treatment, c-CeO_2 nanoparticles were obtained by centrifugation. The resultant nanoparticles were washed with ethanol three times and then dried at 60 °C overnight.

Preparation of o-CeO_2@SiO_2 and o-CeO_2@SiO_2−NH_2. The uniform coating of o-CeO_2 nanoparticles with SiO_2 layer was performed with a slightly modified protocol.[13] o-CeO_2 nanoparticles (100 mg) were dispersed in the mixture of 80 mL of ethanol and 20 mL of DI water. Then 1 mL of concentrated ammonia solution (28 wt %) was added into the above solution under sonication. After that, 45 μL of tetraethyl orthosilicate (TEOS) was added dropwise into the above solution and the mixture was allowed to react for 6 h under magnetic stirring. The as prepared o-CeO_2@SiO_2 nanoparticles were collected by centrifugation. The nanoparticles were washed with water and ethanol for several times before drying at 60 °C overnight. To functionalize o-CeO_2@SiO_2 nanoparticles with amino groups, 25 mg of the above prepared o-CeO_2@SiO_2 was dispersed in 25 mL of absolute isopropyl alcohol under sonication. The obtained slurry was heated to 85 °C and then 100 μL of 3-aminopropyltriethoxysilane (APTES) was added into the slurry. Finally, the mixture was allowed to react for 6 h under vigorous mechanical stirring. The o-CeO_2@SiO_2−NH_2 nanoparticles were centrifuged and washed with water and ethanol three times, respectively.

Preparation of c-CeO_2−COOH. The functionalization of c-CeO_2 nanoparticles with poly(acrylic acid) (PAA) was carried out by the ligand-exchange reactions.[35] Typically, 300 mg of PAA-3000 and 30 mL of diethylene glycol were added into a three-necked flask (150 mL) and the mixture was heated to 110 °C with vigorous stirring under argon atmosphere. Toluene solution of c-CeO_2 nanoparticles (2 mL, 50 mg/mL) was injected dropwise in to the flask and the temperature was kept at 110 °C for 1 h. After that, the solution was heated to 240 °C and allowed to react for 1.5 h. After cooling to room temperature, 30 mL of ethanol was added into the solution to precipitate the nanoparticles. The c-CeO_2−COOH was recovered by centrifugation and then washing the precipitate with water three times.

Construction of the Core−Shell−Satellite Supersandwich Structure. The c-CeO_2−COOH nanoparticles with carboxylic groups was conjugated with the amino groups functionalized CeO_2@SiO_2 by forming amide bond via the classic EDC-NHS coupling. The −COOH groups on c-CeO_2−COOH were activated by EDC/NHS first before the conjugation. Typically, 25 mg of c-CeO_2−COOH was dispersed into 20 mL of 2-(N-morpholino) ethanesulfonic acid (MES) buffer (10 mM, pH = 5.5), and then 10 mM carbodiimide-HCl (EDC) and 25 mM *N*-hydroxysuccinimide (NHS) were added into the above solution. The mixture was incubated at 30 °C for 15 min under shaking. After centrifugation and washing with water, c-CeO_2−COOH nanoparticles were redisposed in 20 mL of PBS buffer (10 mM, pH = 7.2) and then 50 mg of CeO_2@SiO_2−NH_2 nanoparticles was quickly added into the solution under sonication. The solution was allowed to react at 30 °C for 12 h under gentle shaking. The o-CeO_2@SiO_2@c-CeO_2 core−shell−satellite supersandwich nanoparticles were obtained by centrifugation.

Preparation of o-CeO_2@SiO_2@c-CeO_2/Au Supersandwich Nanocomposites. Deposition of Au nanoparticles on o-CeO_2@SiO_2@c-CeO_2 nanoparticles was performed according to a previously reported method.[36] The o-CeO_2@SiO_2@c-CeO_2 nanoparticles (40 mg) were dispersed in 60 mL of water under stirring and then $(NH_4)_2CO_3$ was added into the solution to keep the pH value at 8−9 during the whole process. Aqueous solution of $HAuCl_4$ (70 μL, 48 mM) was then added dropwise into the solution, and the obtained mixture was stirred at 60 °C for 2 h. The resulting precipitate was aged at 60 °C for another 1 h. The precipitate was then filtered and washed with water three times. The obtained yellow powder (o-CeO_2@SiO_2@c-CeO_2/Au) was dried at 70 °C overnight and then calcined at 400 °C for 3 h.

Catalytic Activities of c-CeO_2 and o-CeO_2@SiO_2@c-CeO_2. Acetate buffer solutions with different pH values (pH = 4, 5, 6, 7) were prepared. A 96-well plate was used as the reaction vessel. Typically, 200 μL of acetate buffer, 10 μL of c-CeO_2 or o-CeO_2@SiO_2@c-CeO_2 nanoparticle dispersions (0.5 mg/mL), and 20 μL of dye solution (3,3′,5,5′-tetramethylbenzidine (TMB) in ethanol or 2,2′-azinobis(3-ethylbenzthiazoline-6-sulfonate) (ABTS) in water (0.04 mM)) were added into the corresponding well with six parallel groups for each pH value. Reactions were monitored by recording the characteristic absorption spectrum of TMB or ABTS.

NIR Light Manipulated Photocatalytic Reactions. The NIR light-drived reaction was conducted in a 15 mL quartz test tube under argon atmosphere. The temperature of the reaction system was kept at 40 °C with water bath. A NIR laser with a power density of 20 W/cm^2 was used as the light source. Typically, 10 mg of catalyst, 50 mmol of aromatic nitro compounds, and 1 mL of KOH solution (0.1 M in isopropyl alcohol) were added into 5 mL of isopropyl alcohol. The obtained solution was irradiated with the NIR laser under stirring during the reaction. The azo nitro compounds were analyzed using an

DOI: 10.1021/acsami.5b05633
ACS Appl. Mater. Interfaces 2015, 7, 19416−19423

UV−vis spectrometer and gas chromatography−mass spectrometry (GC-MS).

RESULTS AND DISCUSSION

The structural properties and luminescent feature of o-CeO_2 were thoroughly studied. Transmission electron microscopy (TEM) (Figure 1a,b and Supporting Information, Figure S1)

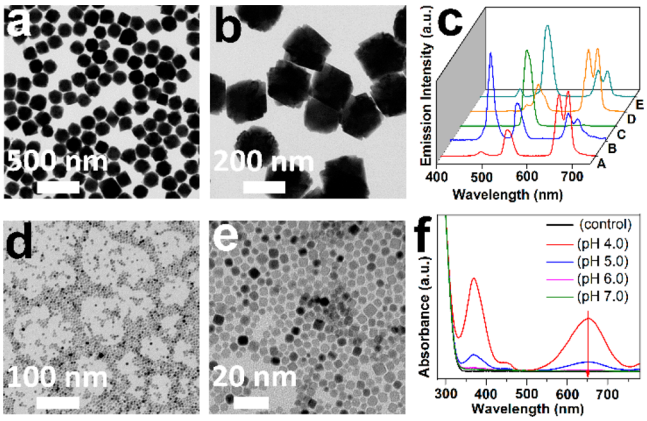

Figure 1. TEM images of o-CeO_2 nanoparticles at different magnifications (a, b). (c) Upconversion luminescence spectra of o-CeO_2 with different dopants (A, $Yb^{3+}/Er^{3+}/Tm^{3+}$: 20/0.5/1 mol %; B, Yb^{3+}/Tm^{3+}: 5/0.5 mol %; C, Yb^{3+}/Ho^{3+}: 5/0.2 mol %; D, Yb^{3+}/Er^{3+}: 10/2 mol %; E, Yb^{3+}/Er^{3+}: 1/2 mol %) (λ_{ex} = 980 nm, power = 5 W). (d, e) TEM images of c-CeO_2 nanoparticles at different magnifications. (f) Catalytic activity of c-CeO_2 toward TMB at different pH values.

and scanning electron microscopy (SEM) (Figure S2) images at different magnification showed that lanthanide ions doped CeO_2 nanoparticles were monodispersed with uniform octahedral shape. The average diameters of these large o-CeO_2 nanoparticles were measured to be about 200 nm based on the above TEM images. Energy dispersive X-ray spectroscopy (EDX) demonstrated the successful doping of the lanthanide ions in the above o-CeO_2 nanoparticles (Figure S3). X-ray diffraction (XRD) pattern indicated that the lanthanide ions doped o-CeO_2 nanoparticles showed typical cube fluorite CeO_2 structure (JCPDF 34-0394), and the strong and sharp diffraction peaks suggested the good crystallinity of the as-prepared nanoparticles (Figure S4).[37] Figure 1c represents the upconversion luminescence spectrum of o-CeO_2 nanoparticles. It is noteworthy that the emission bands of CeO_2 based upconversion nanomaterials can be fine-tuned through simply changing the types and amounts of doped ions, indicating the great flexibility of this upconversion luminescent materials for multiple luminescence related applications. The tiny c-CeO_2 nanoparticles were prepared with a previously reported classic synthetic approach,[34] and their structural and catalytic properties were systematically investigated. As revealed by TEM images, the c-CeO_2 were well-dispersed with average sizes of about 8 nm (Figure 1d, e and Figure S6). XRD analysis shows that the positions of all diffraction peaks were in good agreement with the calculated values (Figure S7). To investigate the catalytic performance of this tiny c-CeO_2, reaction catalyzed by CeO_2 nanoparticles was performed according to a previously reported strategy.[38] As shown in Figures 1f and S8, in the presence of c-CeO_2 nanoparticles, TMB can be oxidized and the solution showed absorption bands at around 370 and 650 nm due to the cation radical produced in the reaction. It was obvious that the adsorption intensity decreased with the increase of pH values, showing the pH-dependent oxidase-like activity of c-CeO_2 nanoparticles. Such pH-dependent activities provide c-CeO_2 with great promise to be used as mild catalyzers, pH-based sensor or even drugs.[39]

As mentioned above, coating nanoparticles-based phosphors with a layer of inert shell would greatly improve the luminescence quantum yields.[31,32] To test whether the luminescence intensities of CeO_2-based upconversion nanoparticles could be enhanced with this strategy, o-CeO_2 nanoparticles were incorporated with a thin layer of silica (designated as o-CeO_2@SiO_2) through the classic sol−gel process by using TEOS as the silicon source.[13] TEM images clearly showed that o-CeO_2@SiO_2 nanoparticles were well dispersed (Figures 2a and S9). At higher magnification (Figures

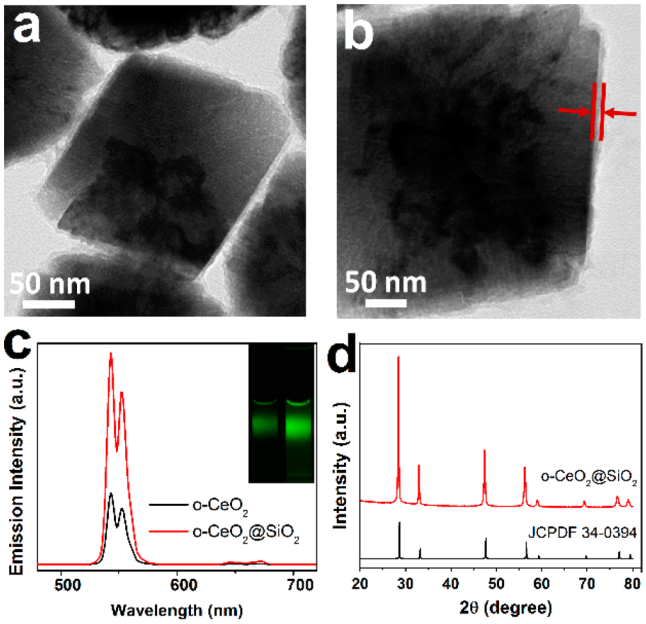

Figure 2. TEM images of o-CeO_2@SiO_2 core−shell structure at different magnifications (a, b). (c) Upconversion luminescence spectra of o-CeO_2 and o-CeO_2@SiO_2 (λ_{ex} = 980 nm, power = 5 W). (d) XRD patterns of o-CeO_2@SiO_2.

2b and S9g−i), a thin layer of SiO_2 (about 2 nm) on the surface of o-CeO_2 nanoparticles was observed. The upconversion luminescent spectrum of o-CeO_2 and o-CeO_2@SiO_2 were presented in Figure 2c. It indicated that SiO_2 shell significantly enhanced the emission intensity of o-CeO_2. The quantum yields of o-CeO_2 and o-CeO_2@SiO_2 nanoparticles were further quantified with the method reported by Prasad and coworkers.[40] The upconversion quantum yields were determined to be 0.028% and 0.053% for o-CeO_2 and o-CeO_2@SiO_2, respectively, clearly suggesting that the SiO_2 shell improved the quantum yield of o-CeO_2. XRD pattern of the o-CeO_2@SiO_2 nanoparticles showed that all of the positions of diffraction peaks were in good agreement with the calculated values (Figure 2d).[41] Additionally, the upconversion mechanism of o-CeO_2 and o-CeO_2@SiO_2 nanoparticles were investigated by measuring the pump power dependence of upconversion emission of these two particles. The emission intensities of both o-CeO_2 and o-CeO_2@SiO_2 nanoparticles increase gradually with the increase of the pump power of the NIR

DOI: 10.1021/acsami.5b05633
ACS Appl. Mater. Interfaces 2015, 7, 19416−19423

light (Figure S11a, b). The pump power dependence of upconversion emission in these two nanoparticles was presented in Figure S11c, d. The slope value represents the number of pump photons absorbed per short wavelength photon emitted. All of the slope values are between 1 and 2, suggesting a two-photon upconversion process is involved to generate the upconversion emissions in both o-CeO_2 and o-CeO_2@SiO_2 nanoparticles.[37]

The strategy to prepare core−shell-satellite supersandwich structure based on CeO_2 nanoparticles with different sizes was illustrated in Figure 3a. Amino groups were introduced to the surface of o-CeO_2@SiO_2 nanoparticles (designated as o-CeO_2@SiO_2−NH_2) through the hydrolysis of 3-aminopropyltriethoxysilane (APTES). The small c-CeO_2 nanoparticles were functionalized with PAA by a ligand-exchange procedure to introduce carboxy functional groups to their surface (designated as c-CeO_2−COOH).[35] The c-CeO_2−COOH nanoparticles were homogeneously assembled on the surface of o-CeO_2@SiO_2 nanoparticles to form the core−shell-satellite supersandwich structure (designated as o-CeO_2@SiO_2@c-CeO_2) with aid of the classic EDC/NHS chemistry. Both o-CeO_2@SiO_2−NH_2 and c-CeO_2−COOH nanoparticles were well dispersed and no morphology changes were observed after modification (Figures S12 and S13). Surface functionalization

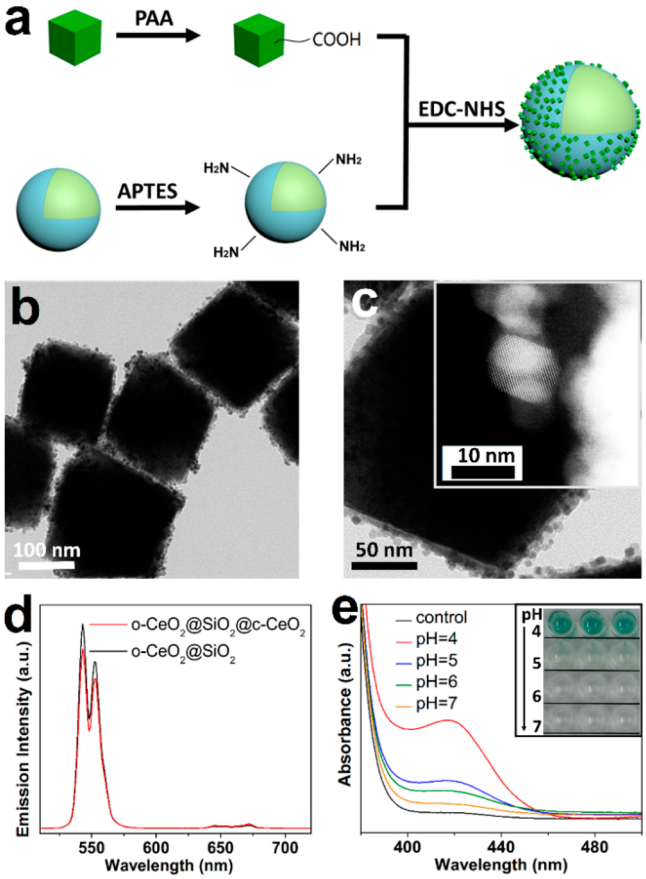

Figure 3. (a) Schematic illustration of the construction of core−shell−satellite supersandwich structure. TEM images of core−shell−satellite nanoparticles with lower (b) and higher (c) magnification. Inset in (c) is the HAADF-STEM image of o-CeO_2@SiO_2@c-CeO_2. (d) Upconversion luminescence spectra of c-CeO_2@SiO_2 and o-CeO_2@SiO_2@c-CeO_2 (λ_{ex} = 980 nm, power = 5 W). (e) Catalytic activity of o-CeO_2@SiO_2@c-CeO_2 toward ABTS at different pH values.

of o-CeO_2@SiO_2 with amino groups and c-CeO_2 with carboxy groups were characterized with Fourier transform infrared spectroscopy (Figure S14). For o-CeO_2@SiO_2−NH_2, the band at around 1630 cm^{-1} corresponded to amine N−H bending and a peak at around 1380 cm^{-1} was due to the internal vibration of amide bonds, which indicated the successful surface modification steps. As for c-CeO_2−COOH, the characteristic stretching vibrations of the C═O group at 1730 cm^{-1} indicate the existence of carboxy groups. Additionally, zeta potential measurements confirmed the presence of amino groups on the surface of o-CeO_2@SiO_2−NH_2 nanoparticles, and the negative charge of c-CeO_2−COOH nanoparticles also demonstrated the successful surface modification of c-CeO_2 with PAA (Figure S15). The structure of core−shell−satellite supersandwich nanocomposites formed by o-CeO_2@SiO_2−NH_2 and c-CeO_2−COOH nanoparticles were thoroughly studied with TEM and high angle annular dark field scanning transmission electron microscopy (HAADF-STEM). TEM images at different magnifications clearly showed that the surfaces of o-CeO_2@SiO_2 were homogeneously decorated with a layer of tiny nanocubes (Figures 3b,c and S16). High resolution TEM and HAADF-STEM images (Figures S17 and S18) implied the attachment of c-CeO_2 nanoparticles on the SiO_2 layer, and the exposed crystallographic planes of c-CeO_2 nanoparticles were well resolved. The luminescent spectrum of the supersandwich core−shell-satellite nanoparticles was shown in Figure 3d. Compared to o-CeO_2@SiO_2 nanoparticles. The slightly decreased luminescent intensity of o-CeO_2@SiO_2@c-CeO_2 suggests that o-CeO_2@SiO_2@c-CeO_2 could also serve as good upconversion luminescent material. Apart from the upconversion properties, o-CeO_2@SiO_2@c-CeO_2 also possessed catalytic function due to the external c-CeO_2 nanoparticles. To test the catalytic activity of this supersandwich structure, ABTS, which could be oxidized and displayed green color in the presence of CeO_2 nanoparticles, was used as the indicator.[38] The absorbance of the reaction solution was monitored in the range of 380−500 nm. As shown in Figure 3e, o-CeO_2@SiO_2@c-CeO_2 still exhibited excellent pH-dependent oxidase-like activity and the catalytic activity became stronger at lower pH conditions. Therefore, one can safely draw the conclusion that the core−shell−satellite perfectly integrated the enhanced upconversion property and pH-dependent catalytic function of CeO_2 within a single nanoparticles. We anticipate these supersandwich core−shell−satellite nanoparticles finding applications various fields. First, the upconversion cores provided the nanostructures with potential to be used in fields such as bioimaging, sensing, and prevention of counterfeiting. Second, the catalytic satellite c-CeO_2 nanoparticles made the nanostructures suitable for serving as catalysts and even biomimic catalyst-based drugs.[41,42] Finally, the upconversion and catalytic functionality can be further utilized simultaneously to achieve more complicated tasks, such as photomanipulated catalysis and indicating the progress of chemical reactions.

As the percentage of NIR light in the solar spectrum was about 44%,[43] efficient utilization of NIR light was of paramount importance in consideration of the global energy shortage. Since o-CeO_2@SiO_2@c-CeO_2 simultaneously possessed upconversion property and catalysis-related function, the utilization of this core−shell−satellite supersandwich nanoparticles as NIR light manipulated photocatalyst was investigated. Aromatic azo compounds are widely used as dyes, food additives, and drugs. The traditional synthesis methods for aromatic azo compounds usually generates a considerable

DOI: 10.1021/acsami.5b05633
ACS Appl. Mater. Interfaces 2015, 7, 19416−19423

amount of byproducts and the reactions are often conducted under harsh or environmentally unfriendly conditions. Previously, Corma developed an innovative strategy to selectively synthesize aromatic azo compounds from anilines and nitroaromatics by using CeO_2 supported gold nanoparticles as the catalyst.[44] Very recently, Zhu and co-workers further reported the selective conversion of aromatic nitro compounds into aromatic azo compounds under visible light irradiation by using CeO_2 supported gold nanoparticles as the photocatalyst, which greatly facilitated the green synthesis of aromatic azo compounds.[45] These studies clearly indicated that CeO_2 nanoparticles could play important roles in the synthesis of aromatic azo compounds.

The selective reduction of aromatic nitro compounds into aromatic azo compounds under NIR light irradiation was conducted by using o-CeO_2@SiO_2@c-CeO_2 based composite nanoparticles as the photocatalyst. To achieve the NIR light manipulated catalytic reaction, gold nanoparticles were loaded on the surface of o-CeO_2@SiO_2@c-CeO_2 (designated as o-CeO_2@SiO_2@c-CeO_2/Au).[36,46] The mechanism of the NIR light manipulated catalytic reaction is illustrated in Scheme 1.

Scheme 1. Schematic Representation of the NIR Light Manipulated Reduction of Aromatic Nitro Compounds to Corresponding Azo Compounds with o-CeO_2@SiO_2@c-CeO_2/Au Supersandwich Nanocomposites

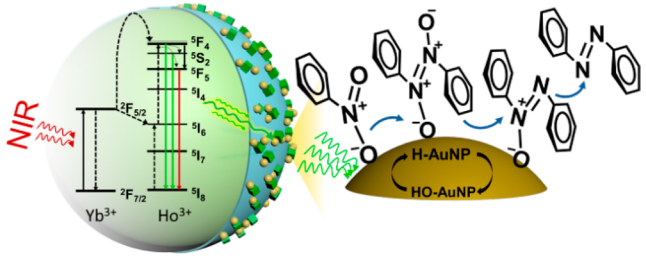

Yb^{3+} and Ho^{3+} doped o-CeO_2 core can absorb NIR photons and emit green light via a nonlinear optical process. Then the emitted green light is absorbed by gold nanoparticles supported on the small c-CeO_2, and the activated gold nanoparticles can thus catalyze the selective conversion of surface adsorbed aromatic nitro compounds into aromatic azo compounds.

The as prepared o-CeO_2@SiO_2@c-CeO_2/Au nanocomposites were thoroughly characterized by TEM, HAADF-STEM, EDX, and XRD analysis. As shown in Figure 4a, the deposited Au nanoparticles were homogeneously distributed on the surface of the nanoparticles with average sizes of about 5 nm. HAADF-STEM images (Figures 4b and S22d) clearly show that gold nanoparticles were well dispersed throughout the surface, leading to rough surface morphology of the entire nanoparticle. At higher magnification (Figures 4c and S22e, f), one could clearly see that gold nanoparticles were attached to the surface of small c-CeO_2, which perfectly formed the c-CeO_2 supported gold nanoparticles catalyst as discussed. EDX analysis demonstrated the existence of Ce, O, Si, and Au in the o-CeO_2@SiO_2@c-CeO_2/Au nanocomposites (Figure S23). Elemental mapping images (Figures 4d–g and S24) clearly suggest the layer-by-layer structure of o-CeO_2@SiO_2@c-CeO_2/Au nanocomposites. In the XRD spectrum (Figure S25), in addition to the diffraction peaks that were preserved due to the CeO_2 component, the other peaks could be well indexed to the typical crystallographic planes of gold nanoparticles. All of these

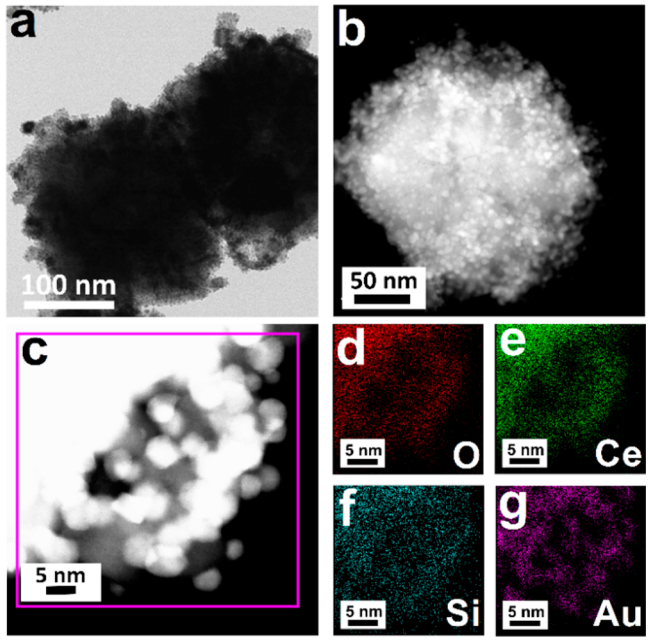

Figure 4. TEM (a) and HAADF-STEM (b) images of o-CeO_2@SiO_2@c-CeO_2/Au nanocomposites. (c) HAADF-STEM image of the edge on an o-CeO_2@SiO_2@c-CeO_2/Au nanoparticle. (d–g) Elemental mapping images of oxygen, cerium, silicon, and gold on the region shown in (c).

results clearly demonstrated the successful construction of the o-CeO_2@SiO_2@c-CeO_2/Au supersandwich photocatalyst.

The performance of this composite photocatalyst in the catalytic reduction of aromatic nitro compounds was further investigated. The luminescent feature of the nanocomposites was investigated first to test whether the green light emitted by central large o-CeO_2 could be absorbed by the outside gold nanoparticles. As shown in Figure 5a, o-CeO_2@SiO_2@c-CeO_2/Au nanoparticles showed a strong absorption band at around 520 nm,[47] and the upconversion emission band of this o-CeO_2@SiO_2@c-CeO_2 also centered at around this wavelength. As expected, the luminescent intensity of o-CeO_2@SiO_2@c-CeO_2 was significantly decreased after the deposition of gold nanoparticles, which resulted from the well matched absorption band of gold nanoparticles and the emission peak of large o-CeO_2 nanoparticles. Aromatic nitro compound nitrobenzene was chosen as the substrate and isopropyl alcohol as the solvent and hydrogen donor to test the photocatalytic activity of o-CeO_2@SiO_2@c-CeO_2/Au.[48] The reaction process was monitored by GC-MS. As shown in Figure 5b, the concentration of nitrobenzene decreased gradually. On the other hand, the amounts of azobenzene increased gradually, suggesting the selective reduction of nitrobenzene to azobenzene under the irradiation of NIR light. After about 48 h, nitrobenzene was almost completely converted to azobenzene. The conversion rate of nitrobenzene was determined to be over 99% with ultrahigh selectivity (98%), clearly demonstrating the great promise of o-CeO_2@SiO_2@c-CeO_2/Au for serving as photocatalyst in the selective reduction of aromatic azo compounds. Furthermore, azoxybenzene was formed during the reaction, with concentration increased first and then gradually decreased to zero as the reaction proceeded, which indicated that azoxybenzene was serve as the intermediate product in this reaction.[48] Photographs of the reaction solutions at different time intervals is shown in Figure 5c. It was observed that the

DOI: 10.1021/acsami.5b05633
ACS Appl. Mater. Interfaces 2015, 7, 19416–19423

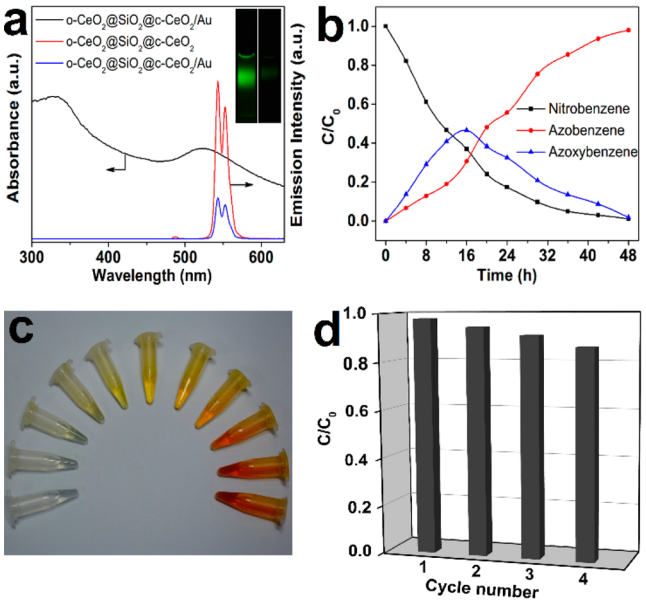

Figure 5. (a) Upconversion luminescence spectra of o-CeO_2@SiO_2 @ c-CeO_2 and o-CeO_2@SiO_2@c-CeO_2/Au (λ_{ex} = 980 nm, power = 5 W); UV−vis absorption spectra of o-CeO_2@SiO_2@c-CeO_2/Au. Inset: luminescent photographs of o-CeO_2@SiO_2@c-CeO_2 and o-CeO_2@SiO_2@c-CeO_2/Au under excitation of NIR laser. (b) Time courses for nitrobenzene reduction by o-CeO_2@SiO_2@c-CeO_2/Au. C is the concentration at the irradiation time t, and C_0 is the original concentration. (c) Photographs of the reaction solution at different time intervals. (d) Recycling photocatalytic reduction of nitrobenzene over o-CeO_2@SiO_2-c-CeO_2/Au under NIR light irradiation.

solution showed continuous color change with the gradual conversion of nitrobenzene to azobenzene. One step further, the reusability of the composite photocatalyst was investigated. As presented in Figure 5d, CeO_2@SiO_2@c-CeO_2/Au was reused four times and no appreciable loss of its catalytic activity was observed. TEM images also suggested that no obvious morphology changes of CeO_2@SiO_2@c-CeO_2/Au nanocomposites were observed in the recycling tests (Figure S27), implying the promise of this composite catalyst for practical catalytic applications. Control experiments were also conducted to test the catalytic performance of o-CeO_2@SiO_2, o-CeO_2@SiO_2@c-CeO_2, o-CeO_2@SiO_2/Au (gold nanoparticles deposited on the surface of o-CeO_2@SiO_2, Figure S28), and o-CeO_2@SiO_2@c-CeO_2−Au (the mixture of o-CeO_2@SiO_2@c-CeO_2 and gold nanoparticles) under the excitation of NIR light. The o-CeO_2@SiO_2 and o-CeO_2@SiO_2@c-CeO_2 nanoparticles displayed no catalytic activities, while o-CeO_2@SiO_2/Au and o-CeO_2@SiO_2@ c-CeO_2−Au nanocomposites showed modest catalytic activities with conversion rates of about 33.41% and 39.30%, respectively (Table S1). These control tests clearly demonstrated the essential role that c-CeO_2/Au (c-CeO_2 supported gold nanoparticles) played in the catalytic reaction. The above results clearly suggested that o-CeO_2@SiO_2@c-CeO_2/Au could efficiently utilize NIR light for the selective reduction of aromatic nitro compounds to aromatic azo compounds.

Furthermore, 1-chloro-4-nitrobenzene and 4-nitrotoluene were also utilized as the substrates to test the general applicability of the o-CeO_2@SiO_2@c-CeO_2/Au nanocomposites. As shown in Table 1, these two aromatic nitro compounds could also be efficiently converted to the corresponding azo compounds under the irradiation of NIR light with conversion rates of 68.77% and 83.21%, respectively. It is noteworthy that the selectivities of o-CeO_2@SiO_2@c-CeO_2/Au photocatalyst toward these two compounds were all above 85%. These results therefore serve to demonstrate the general applicability of the composite photocatalyst for selective reduction of aromatic nitro compounds into corresponding azo compounds.

Table 1. NIR-Driven Reduction of Nitroaromatic Compounds by Using o-CeO_2@SiO_2@c-CeO_2/Au as the Photocatalyst[a]

substrate	T [°C]	t [h]	conv [%]	selec [%]
4-nitrotoluene	40	48	68.77	84.59
1-chloro-4-nitrobenzene	40	48	83.21	89.65

[a]conv = conversion, selec = selectivity.

CONCLUSIONS

In summary, we have highlighted the creation of a novel single component based core−shell−satellite supersandwich structure with NIR light manipulated catalytic activity. The supersandwich nanoparticles simultaneously possessed upconversion luminescent and catalytic functionality, suggesting their potential applications in luminescence and catalysis related areas. It was noteworthy that the upconversion quantum yield of lanthanide-doped CeO_2 nanoparticles was nearly doubled. Furthermore, the supersandwich nanostructure was deposited with gold nanoparticles, with the performance of the supersandwich nanocomposites in the catalytic reduction of aromatic nitro compounds to aromatic azo compounds thoroughly investigated. The nanocomposites exhibited good catalytic activity and it can be easily recycled for several times without significant loss of activity. To conclude, the strategy described here not only can serve as a universal method for the construction of functional super structures, but also can further expand the applications of ceria based materials in green catalysis, bioimaging, and biomedicine.

ASSOCIATED CONTENT

Supporting Information

The Supporting Information is available free of charge on the ACS Publications website at DOI: 10.1021/acsami.5b05633.

Additional information, including SEM, TEM, STEM, XRD, and EDX characterization, zeta potentials, UV−vis, FTIR and fluorescence spectra, electron energy loss spectroscopy, additional detailed catalytic results, pump power dependences of upconversion emissions in o-CeO_2 and o-CeO_2@SiO_2, methods for quantification of upconversion quantum yields, application explorations, chemicals, and instruments (PDF)

AUTHOR INFORMATION

Corresponding Author

*E-mail: yuanquan@whu.edu.cn.

Notes

The authors declare no competing financial interest.

ACKNOWLEDGMENTS

This work was supported by the National Natural Science Foundation of China (21201133, 51272186, 21422105). Q.Y. thanks the large-scale instrument and equipment sharing foundation of Wuhan University.

DOI: 10.1021/acsami.5b05633
ACS Appl. Mater. Interfaces 2015, 7, 19416−19423

REFERENCES

(1) Haase, M.; Schafer, H. Upconverting Nanoparticles. *Angew. Chem., Int. Ed.* **2011**, *50*, 5808−5829.
(2) Wang, F.; Liu, X. G. Recent Advances in the Chemistry of Lanthanide-Doped Upconversion Nanocrystals. *Chem. Soc. Rev.* **2009**, *38*, 976−989.
(3) Gai, S. L.; Li, C. X.; Yang, P. P.; Lin, J. Recent Progress in Rare Earth Micro/Nanocrystals: Soft Chemical Synthesis, Luminescent Properties, and Biomedical Applications. *Chem. Rev.* **2014**, *114*, 2343−2389.
(4) Sato, S.; Sato, F.; Gotoh, H.; Yamada, Y. Selective Dehydration of Alkanediols into Unsaturated Alcohols over Rare Earth Oxide Catalysts. *ACS Catal.* **2013**, *3*, 721−734.
(5) Wu, Y. E.; Wang, D. S.; Li, Y. D. Nanocrystals from Solutions: Catalysts. *Chem. Soc. Rev.* **2014**, *43*, 2112−2124.
(6) Gangopadhyay, S.; Frolov, D. D.; Masunov, A. E.; Seal, S. Structure and Properties of Cerium Oxides in Bulk and Nanoparticulate Forms. *J. Alloys Compd.* **2014**, *584*, 199−208.
(7) Fernandez-Garcia, M.; Martinez-Arias, A.; Hanson, J. C.; Rodriguez, J. A. Nanostructured Oxides in Chemistry: Characterization and Properties. *Chem. Rev.* **2004**, *104*, 4063−4104.
(8) Yamada, Y.; Tsung, C.-K.; Huang, W. Y.; Huo, Z. Y.; Ha bas, S. E.; Soejima, T.; Aliaga, C. E.; Somorjai, G. A.; Yang, P. D. Nanocrystal Bilayer for Tandem Catalysis. *Nat. Chem.* **2011**, *3*, 372−376.
(9) Li, G. D.; Tang, Z. Y. Noble Metal Nanoparticle@Metal Oxide Core/Yolk−Shell Nanostructures as Catalysts: Recent Progress and Perspective. *Nanoscale* **2014**, *6*, 3995−4011.
(10) Wang, D. G.; Chen, H. C.; Chang, G. L.; Lin, X.; Zhang, Y. Y.; Aldalbahi, A.; Peng, P.; Wang, J. Q.; Fan, C. H. Uniform Doping of Titanium in Hematite Nanorods for Efficient Photoelectrochemical Water Splitting. *ACS Appl. Mater. Interfaces* **2015**, *7*, 14072−14078.
(11) Zhou, J.; Liu, Z.; Li, F. Y. Upconversion Nanophosphors for Small-Animal Imaging. *Chem. Soc. Rev.* **2012**, *41*, 1323−1349.
(12) Coti, K. K.; Belowich, M. E.; Liong, M.; Ambrogio, M. W.; Lau, Y. A.; Khatib, H. A.; Zink, J. I.; Khashab, N. M.; Stoddart, J. F. Mechanised Nanoparticles for Drug Delivery. *Nanoscale* **2009**, *1*, 16−39.
(13) Deng, Y. H.; Cai, Y.; Sun, Z. K.; Liu, J.; Liu, C.; Wei, J.; Li, W.; Liu, C.; Wang, Y.; Zhao, D. Y. Multifunctional Mesoporous Composite Microspheres with Well-Designed Nanostructure: A Highly Integrated Catalyst System. *J. Am. Chem. Soc.* **2010**, *132*, 8466−8473.
(14) Li, K.; Wang, K.; Qin, W. W.; Deng, S. H.; Di, L.; Shi, J. Y.; Huang, Q.; Fan, C. H. DNA-Directed Assembly of Gold Nano-Halo for Quantitative Plasmonic Imaging of Single-Particle Catalysis. *J. Am. Chem. Soc.* **2015**, *137*, 4292−4295.
(15) Ruan, Q. F.; Shao, L.; Shu, Y. W.; Wang, J. F.; Wu, H. K. Growth of Monodisperse Gold Nanospheres with Diameters from 20 to 220 nm and Their Core/Satellite Nanostructures. *Adv. Opt. Mater.* **2014**, *2*, 65−73.
(16) Carrettin, S.; Concepción, P.; Corma, A.; Lopez Nieto, J. M.; Puntes, V. F. Nanocrystalline CeO_2 Increases the Activity of Au for CO Oxidation by Two Orders of Magnitude. *Angew. Chem., Int. Ed.* **2004**, *43*, 2538−2540.
(17) Fu, Q.; Saltsburg, H.; Flytzani-Stephanopoulos, M. Active Nonmetallic Au and Pt Species on Ceria-Based Water-Gas Shift Catalysts. *Science* **2003**, *301*, 935−938.
(18) Paier, J.; Penschke, C.; Sauer, J. Oxygen Defects and Surface Chemistry of Ceria: Quantum Chemical Studies Compared to Experiment. *Chem. Rev.* **2013**, *113*, 3949−3895.
(19) Loschen, C.; Bromley, S. T.; Neyman, K. M.; Illas, F. Understanding Ceria Nanoparticles from First-Principles Calculations. *J. Phys. Chem. C* **2007**, *111*, 10142−10145.
(20) Liu, X. W.; Zhou, K. B.; Wang, L.; Wang, B. Y.; Li, Y. D. Oxygen Vacancy Clusters Promoting Reducibility and Activity of Ceria Nanorods. *J. Am. Chem. Soc.* **2009**, *131*, 3140−3141.
(21) Dutta, P.; Pal, S.; Seehra, M. S.; Shi, Y.; Eyring, E. M.; Ernst, R. D. Concentration of Ce^{3+} and Oxygen Vacancies in Cerium Oxide Nanoparticles. *Chem. Mater.* **2006**, *18*, 5144−5146.
(22) Lawrence, N. J.; Brewer, J. R.; Wang, L.; Wu, T.-S.; Wells-Kingsbury, J.; Ihrig, M. M.; Wang, G.; Soo, Y.-L.; Mei, W.-N.; Cheung, C. L. Defect Engineering in Cubic Cerium Oxide Nanostructures for Catalytic Oxidation. *Nano Lett.* **2011**, *11*, 2666−2671.
(23) Liu, Y. S.; Tu, D. T.; Zhu, H. M.; Chen, X. Y. Lanthanide-Doped Luminescent Nanoprobes: Controlled Synthesis, Optical Spectroscopy, and Bioapplications. *Chem. Soc. Rev.* **2013**, *42*, 6924−6958.
(24) Wang, Z. L.; Quan, Z. W.; Lin, J. Remarkable Changes in the Optical Properties of CeO_2 Nanocrystals Induced by Lanthanide Ions Doping. *Inorg. Chem.* **2007**, *46*, 5237−5242.
(25) Kumar, A.; Babu, S.; Karakoti, A. S.; Schulte, A.; Seal, S. Luminescence Properties of Europium-Doped Cerium Oxide Nanoparticles: Role of Vacancy and Oxidation States. *Langmuir* **2009**, *25*, 10998−11007.
(26) Wu, J. J.; Shi, S. K.; Wang, X. L.; Li, J. B.; Zong, R. L.; Chen, W. Controlled Synthesis and Optimum Luminescence of Sm^{3+}-Activated Nano/Submicroscale Ceria Particles by a Facile Approach. *J. Mater. Chem. C* **2014**, *2*, 2786−2792.
(27) Zhang, C. M.; Lin, J. Defect-Related Luminescent Materials: Synthesis, Emission Properties and Applications. *Chem. Soc. Rev.* **2012**, *41*, 7938−7961.
(28) Yuan, Q.; Duan, H.-H.; Li, L.-L.; Sun, L.-D.; Zhang, Y.-W.; Yan, C. H. Controlled Synthesis and Assembly of Ceria-Based Nanomaterials. *J. Colloid Interface Sci.* **2009**, *335*, 151−167.
(29) Fujihara, S.; Oikawa, M. Structure and Luminescent Properties of CeO_2: Rare Earth (RE = Eu^{3+} and Sm^{3+}) Thin Films. *J. Appl. Phys.* **2004**, *95*, 8002−8006.
(30) Han, S. Y.; Deng, R. R.; Xie, X. J.; Liu, X. G. Enhancing Luminescence in Lanthanide-Doped Upconversion Nanoparticles. *Angew. Chem., Int. Ed.* **2014**, *53*, 11702−11715.
(31) Lehmann, O.; Kömpe, K.; Haase, M. Synthesis of Eu^{3+}-Doped Core and Core/Shell Nanoparticles and Direct Spectroscopic Identification of Dopant Sites at the Surface and in the Interior of the Particles. *J. Am. Chem. Soc.* **2004**, *126*, 14935−14942.
(32) Liu, T.; Xu, W.; Bai, X.; Song, H. W. Tunable Silica Shell and Its Modification on Photoluminescent Properties of Y_2O_3:Eu^{3+}@SiO_2 Nanocomposites. *J. Appl. Phys.* **2012**, *111*, 064312.
(33) Chen, G. Z.; Zhu, F. F.; Sun, X.; Sun, S. X.; Chen, R. Benign Synthesis of Ceria Hollow Nanocrystals by a Template-Free Method. *CrystEngComm* **2011**, *13*, 2904−2908.
(34) Liu, X. Y.; Wei, W.; Yuan, Q.; Zhang, X.; Li, N.; Du, Y. G.; Ma, G. H.; Yan, C. H.; Ma, D. Apoferritin−CeO_2 Nano-Truffle that Has Excellent Artificial Redox Enzyme Activity. *Chem. Commun.* **2012**, *48*, 3155−3157.
(35) Wang, J.; Wei, T.; Li, X. Y.; Zhang, B. H.; Wang, J. X.; Huang, C.; Yuan, Q. Near-Infrared-Light-Mediated Imaging of Latent Fingerprints based on Molecular Recognition. *Angew. Chem., Int. Ed.* **2014**, *53*, 1616−1620.
(36) Si, R.; Flytzani-Stephanopoulos, M. Shape and Crystal-Plane Effects of Nanoscale Ceria on the Activity of Au-CeO_2 Catalysts for the Water−Gas Shift Reaction. *Angew. Chem., Int. Ed.* **2008**, *47*, 2884−2887.
(37) Cho, J.-H.; Bass, M.; Babu, S.; Dowding, J. M.; Self, W. T.; Seal, S. Up Conversion Luminescence of Yb^{3+}−Er^{3+} Codoped CeO_2 Nanocrystals with Imaging Applications. *J. Lumin.* **2012**, *132*, 743−749.
(38) Asati, A.; Santra, S.; Kaittanis, C.; Nath, S.; Perez, J. M. Oxidase-Like Activity of Polymer-Coated Cerium Oxide Nanoparticles. *Angew. Chem., Int. Ed.* **2009**, *48*, 2308−2312.
(39) Xu, C.; Lin, Y. H.; Wang, J. S.; Wu, L.; Wei, W. L.; Ren, J. S.; Qu, X. G. Nanoceria-Triggered Synergetic Drug Release Based on CeO_2-Capped Mesoporous Silica Host−Guest Interactions and Switchable Enzymatic Activity and Cellular Effects of CeO_2. *Adv. Healthcare Mater.* **2013**, *2*, 1591−1599.
(40) Chen, G. Y.; Ohulchanskyy, T. Y.; Kachynski, A.; Ågren, H.; Prasad, P. N. Intense Visible and Near-Infrared Upconversion Photoluminescence in Colloidal $LiYF_4$:Er^{3+} Nanocrystals under Excitation at 1490 nm. *ACS Nano* **2011**, *5*, 4981−4986.

DOI: 10.1021/acsami.5b05633
ACS Appl. Mater. Interfaces 2015, 7, 19416−19423

(41) Kang, X. J.; Cheng, Z. Y.; Li, C. X.; Yang, D. M.; Shang, M. M.; Ma, P. A.; Li, G. G.; Liu, N.; Lin, J. Core-Shell Structured Up-Conversion Luminescent and Mesoporous $NaYF_4:Yb^{3+}/Er^{3+}$@ $nSiO_2$@$mSiO_2$ Nanospheres as Carriers for Drug Delivery. *J. Phys. Chem. C* **2011**, *115*, 15801−15811.
(42) Shen, J.; Zhao, L.; Han, G. Lanthanide-Doped Upconverting Luminescent Nanoparticle Platforms for Optical Imaging-Guided Drug Delivery and Therapy. *Adv. Drug Delivery Rev.* **2013**, *65*, 744−755.
(43) Qin, W. P.; Zhang, D. S.; Zhao, D.; Wang, L. L.; Zheng, K. Z. Near-Infrared Photocatalysis Based on $YF_3:Yb^{3+},Tm^{3+}/TiO_2$ Core/Shell Nanoparticles. *Chem. Commun.* **2010**, *46*, 2304−2306.
(44) Grirrane, A.; Corma, A.; García, H. Gold-Catalyzed Synthesis of Aromatic Azo Compounds from Anilines and Nitroaromatics. *Science* **2008**, *322*, 1661−1664.
(45) Ke, X. B.; Zhang, X. G.; Zhao, J.; Sarina, S.; Barry, J.; Zhu, H. Y. Selective Reductions Using Visible Light Photocatalysts of Supported Gold Nanoparticles. *Green Chem.* **2013**, *15*, 236−244.
(46) Xu, X. Y.; Kyaw, A. K. K.; Peng, B.; Du, Q. G.; Hong, L.; Demir, H. V.; Wong, T. K. S.; Xiong, Q. H.; Sun, X. W. Enhanced Efficiency of Solution-Processed Small-Molecule Solar Cells Upon Incorporation of Gold Nanospheres and Nanorods into Organic Layers. *Chem. Commun.* **2014**, *50*, 4451−4454.
(47) Du, Y. P.; Chen, B.; Yin, Z. Y.; Liu, Z. Q.; Zhang, H. Phosphine-Free, Low-Temperature Synthesis of Tetrapod-Shaped CdS and Its Hybrid with Au Nanoparticles. *Small* **2014**, *10*, 4727−4734.
(48) Zhu, H. Y.; Ke, X. B.; Yang, X. H.; Sarina, S.; Liu, H. W. Reduction of Nitroaromatic Compounds on Supported Gold Nanoparticles by Visible and Ultraviolet Light. *Angew. Chem., Int. Ed.* **2010**, *49*, 9657−9661.

DOI: 10.1021/acsami.5b05633
ACS Appl. Mater. Interfaces 2015, 7, 19416−19423